28 THERMAL DETECTORS

William L. Wolfe
College of Optical Sciences
University of Arizona
Tucson, Arizona

Paul W. Kruse
Consultant
Edina, Minnesota

28.1 GLOSSARY

DTGS	deuterated triglycine sulfate
p	pyroelectric coefficient
R_e	electrical resistance
R_{th}	thermal resistance
$\Re$	responsivity
S	Seebeck coefficient
TGS	triglycine sulfate
Z	figure of merit
τ_e	electrical time constant
τ_{th}	thermal time constant

28.2 THERMAL DETECTOR ELEMENTS[1]

Introduction

Thermal detectors (transducers) of optical radiation are generally considered to be those devices that absorb the radiation, increase their own temperature, and provide a resultant electrical signal. There are several types, divided according to the physical mechanism that converts the temperature change to a resultant electrical one. The oldest are bolometers and thermocouples. The bolometer changes its electrical resistance as a result of the temperature increase; the thermocouple changes its contact potential difference. There are several different types of bolometers, including thermistor, semiconducting, superconducting, carbon, and metallic. They may also be subdivided according to whether they operate at room or cryogenic temperature. Thermocouples vary according to the materials that are joined, and are sometimes connected in series to generate thermopiles.

Pyroelectric detectors make use of the property of a change in the internal polarization as a function of the change in temperature, the pyroelectric effect. Golay cells and certain variations make use of the expansion of a gas with temperature. All of these detectors are governed by the fundamental equation of heat absorption in the material. Many reviews and two books of collected reprints[2] provide additional information.

Thermal Circuit Theory

In the absence of joulean heating of the detector element, the spectrum of the temperature difference $d\Delta\tilde{T}$ is given in terms of the spectrum of the absorbed power $\tilde{P}$ (the power is P)

$$d\Delta\tilde{T} = \frac{\epsilon\tilde{P}}{G(1+i\omega\tau)} \tag{1}$$

where G is the thermal conductance, given by the product of the thermal conductivity times the cross-sectional area of the path to the heat sink and divided by the length of the path to that heat sink. The time constant τ is the product of the thermal resistance and the heat capacitance. The thermal resistance is the reciprocal of the thermal conductance, while the thermal capacitance is the thermal capacity times the mass of the detector. In the absence of joulean heating, this is a simple, single time constant thermal circuit, for which the change in temperature is given by

$$d\tilde{T} = \frac{\epsilon\tilde{P}}{G(1+i\omega\tau)} \tag{2}$$

The absorbed power is equal to the incident power times the absorptance α of the material:

$$\tilde{P} = \epsilon\tilde{P}_i \tag{3}$$

The absorptance α is usually written as ϵ (which is legitimate according to Kirchhoff's law) since α is also used for the relative temperature coefficient of resistance (some writers use η).

$$\alpha = \frac{1}{R}\frac{dR}{dT} \tag{4}$$

As radiation is absorbed, part of the heat is conducted to the sink. Some of it gives rise to an increase in temperature. Some is reradiated, but this is usually quite small and is ignored here. The dc responsivity of a thermal detector is proportional to the emissivity and to the thermal resistance. The greater proportion of radiation that is absorbed, the greater will be the responsivity. The less heat that is conducted to the sink, the greater will be the temperature rise. The time constant is a true thermal time constant, the product of thermal resistance and capacitance. The greater the heat capacitance, the more heat necessary for a given temperature increase, and the less heat conducted to the sink, the more available for temperature increase. A high absorptance is accomplished by the use of a black coating, and a sufficient amount of it. Thus, there is a direct conflict between high speed and high responsivity.

The Ideal Thermal Detector[3–6]

The ideal thermal detector has a noise that is associated only with the thermal fluctuations of the heat loss to the heat sink, and this coupling is purely radiative. Then the noise equivalent power (NEP) is given by

$$\text{NEP} = \sqrt{16A\sigma kT^5/\epsilon} \tag{5}$$

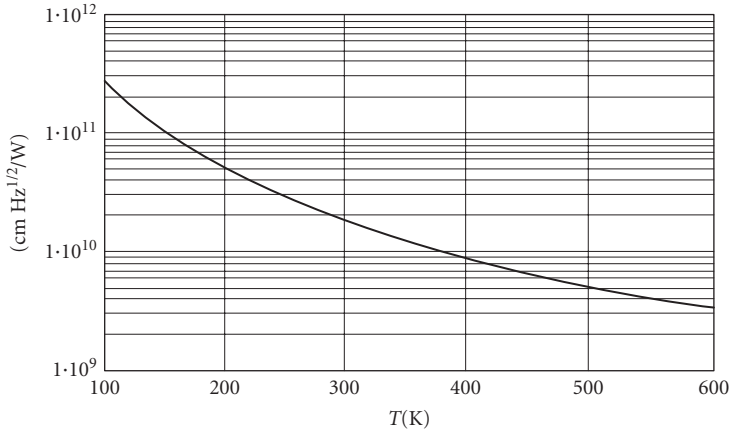

FIGURE 1 Theoretical specific detectivity for ideal thermal detectors.

where it is assumed that the detector is irradiated by a hemisphere of blackbody radiation at the same temperature T as the detector. The corresponding specific detectivity, assuming that the signal varies as the area and the noise as its square root, is

$$D^* = \frac{\epsilon^{1/2}}{4\sqrt{\sigma k T^5}} \tag{6}$$

where the detector and background are at the same temperature.

For circumstances in which the detector is in a cooled chamber, the total radiation from the sources at various temperatures must be calculated. Figure 1 shows the specific detectivity of a background limited ideal thermal detector as a function of the temperature of the surround.

No detector is ideal, and every one will be limited by the signal loss due to incomplete absorption at the surface and any transmission losses by the optical system that puts the radiation on the detector. The detector will also have noise that arises from its conductive coupling to the heat sink, and probably Johnson noise as well. The conductive mean square power fluctuation is given by

$$\langle P^2 \rangle = 4kT^2G \tag{7}$$

The Johnson noise power density is $4kT$. Therefore, the total mean square power fluctuation is given by

$$\langle P^2 \rangle = 4kT[GT + 4\epsilon A\sigma T^4 + 1] \tag{8}$$

Bolometers

Most single-element bolometers are connected in a voltage divider network, as shown in Fig. 2. A stable voltage supply is used to develop a current and consequent voltage drop across the two resistors. One is the detector, while the other should be a matching element to eliminate signals arising from a change in the ambient temperature. It should match the detector in both resistance and in the

temperature coefficient of resistance. Usually another, but blinded, detector is used. The expression for power conservation is

$$C\frac{d\Delta T}{dt}+G\Delta T=\frac{d(i^2R)}{dt}\Delta T+P$$

$$C\frac{d\Delta T}{dt}+G\Delta T=\frac{V^2(R_1-R)}{(R_1+R)^3}\frac{dR}{dT}\Delta T+P \tag{9}$$

$$C\frac{d\Delta T}{dt}+\left[G-\frac{V^2R\alpha}{(R_1+R)^2}\frac{(R_1-R)}{(R_1+R)}\right]\Delta T=P$$

The solution to this is a transient that has an RC time constant, where R is the reciprocal of the bracketed term, and C is the thermal capacitance, and the same steady-state term given above. The transient decays as long as G is greater than the rest of the bracket, but the detector burns up if not. This is still another reason for matching the resistances. The dc responsivity is a function of the construction parameters, including the path to the sink, the bias voltage, and the relative change of resistance with temperature. The different bolometers are divided according to how their resistances change with temperature. (R_1 and R represent slightly different values of R_D.)

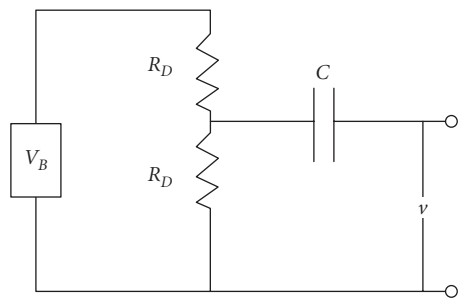

FIGURE 2 Balanced voltage divider circuit for a thermal detector.

Metal Bolometers These have a linear change in resistance with temperature that may be expressed as

$$R=R_0[1+\gamma(T-T_0)] \tag{10}$$

Therefore the thermal coefficient is

$$\alpha=\frac{\gamma}{1+\gamma(T-T_0)} \tag{11}$$

This coefficient always decreases with temperature, and burnout does not occur. The coefficient is approximately equal to the inverse of the temperature, and is therefore never very high.

Semiconductor Bolometers These have an exponential change of resistance with temperature, given by

$$R=R_0e^{\beta/T} \tag{12}$$

so that

$$\alpha=-\beta/T^2 \tag{13}$$

The value of β depends upon the particular material. These detectors can burn out. Two basic types exist: (1) those that are used at low temperatures and (2) those that are used at about room temperature.

The most used low-temperature bolometer[7] is germanium in a bath of liquid helium. Pure germanium is transparent in the infrared, but with enough compensated doping it becomes a good conductor with a high-temperature coefficient of resistance.[8] Typical concentrations are about 10^{16}cm^{-3} of gallium and 10^{15} of indium. Even these are not sufficient at wavelengths shorter than 10 μm since the free-carrier absorption is proportional to wavelength. In such a case a black coating is sometimes used. Improvements have been made since Low's first work.[9–11]

Superconducting Bolometers These make use of the extremely large thermal coefficient of resistance at the transition temperature.[12–14] Originally they needed to be controlled very carefully, or a small change in ambient conditions (on the order of 0.01 K) could cause an apparent signal of appreciable magnitude. A more recent version[15] incorporates an evaporated thin film on an anodized aluminum block that is coupled to a helium bath by a brass rod. The detector has a time constant of about 3 μs due to this high thermal conductance and a good NEP of about 10^{-13} WHz$^{-1/2}$. It still must be controlled to about 10^{-5} K, and this is accomplished with a heater current and control circuit.

Recently developed materials not only have high-temperature transition points but also have more gradual transitions, and provide a better compromise between good responsivity and the requirement for exquisite control.[16]

Carbon Bolometers These are a form of semiconductor bolometers that have been largely superseded by germanium bolometers. They are made of small slabs of carbon resistor material, connected to a metal heat sink by way of a thin mylar film. Although their responsivities are comparable to germanium bolometers, their noise is several orders of magnitude higher.[17]

Thermocouples and Thermopiles[18,19]

A *thermocouple* is made by simply joining two dissimilar conductors. A good pair has a large relative Seebeck coefficient and gives rise to a potential difference. The materials also have large electrical conductivities and small thermal ones, so there is little voltage drop across the length and a small thermal gradient. Although there are many different couples (many are not even used for radiation detection), those most often used for this application are bismuth telluride, copper, and constantan. The expression for the responsivity is given in terms of the relative Seebeck coefficient S_{12} (the difference in the voltage change with temperature between the two materials) and the expression derived above for the thermal circuit

$$\Re = \frac{S\epsilon}{G(1+i\omega\tau)} \tag{14}$$

Good materials are those that have a large Seebeck coefficient, a high electrical conductivity, and a small thermal conductivity, and the figure of merit is often defined as

$$Z_{12} = \frac{S_{12}^2}{\left[\sqrt{G_1/\sigma_1} + \sqrt{G_2/\sigma_2}\right]^2} \tag{15}$$

Thermopiles are arrays of thermocouples connected in series. They are manufactured in two ways. Some are carefully wound wires with junctions aligned in the desired pattern, while others are evaporated with the pattern determined by masking operations. Most of the "bulk" thermopiles are wrapped on appropriate mandrels to obtain rigidity. Both kinds are obtainable in a variety of sizes

and patterns that correspond to such things as spectrometer slits, centering annuli, and staggered arrays for moderate-sensitivity thermal imaging.

The Golay Cell[20]

This detector is used mostly for laboratory operations, as it is slow and fragile, although it has high sensitivity. It is a gas-filled chamber that has a thin membrane at one end and a blackened detector area at the other. Light on the blackened surface causes the increase in temperature; this is transferred to the gas which therefore expands. The membrane bulges, and the amount of the bulge is sensed by some sort of optical lever[21] or even change in capacity of an electrical element.[22] Other versions do not use a blackened surface, but allow the radiation to interact with the gas directly, in which case they are spectral detectors that are "tuned" to the absorption spectrum of the gas.[23]

Pyroelectric Detectors[24]

Some crystals which do not have a center of symmetry experience an electric field along a crystal axis. This internal electric field results from an alignment of electric dipoles (known as polarization), and is related to the crystal temperature. In these ferroelectric crystals, this results in a charge being generated and stored on plates connected to the crystal. Polarization disappears above the so-called Curie temperature that is characteristic of each material. Thus, below the Curie temperature, a change in temperature results in a current. The equation for the response of a pyroelectric detector is

$$\Re = \frac{\omega p A_d \epsilon R_e R_{\text{th}}}{(1+i\omega\tau_{\text{th}})(1+i\omega\tau_e)} \tag{16}$$

where ω is the radian frequency, p is the pyroelectric coefficient, A_d is the detector area, R_e is the electrical resistance, R_{th} is the thermal resistance, τ_{th} is the thermal time constant, and τ_e is the electrical time constant. The relation is shown in Fig. 3, where the responsivity is plotted as a function of frequency. In the low-frequency region the responsivity rises directly as the frequency. This is a result of the ac operation of a pyroelectric. At the (radian) frequency that is the reciprocal of the slower (usually the thermal) time constant, the response levels off. This is the product of the ac rise and the thermal rolloff. Then, when the frequency corresponding to the shorter time constant is reached, the response rolls off.

Type II pyroelectric detectors work on a slightly different mechanism, which is still not fully understood. The electrodes are on the sensing surface of the detector and parallel to the polar axis. In these crystals, the temperature change is not uniform at the onset of radiation and the primary

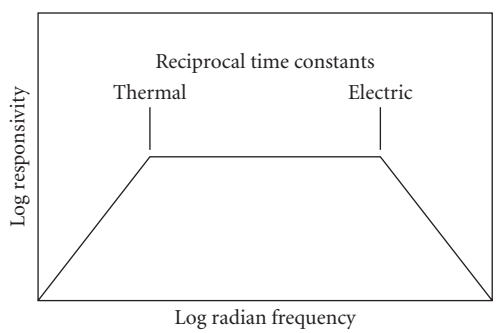

FIGURE 3 Responsivity asymptotes versus frequency.

TABLE 1 General Properties of Thermal Detectors

Type	Operating Temperature (K)	$D^* \times 10^8$ ($cmHz^{1/2}W^{-1}$)	NEP $\times 10^{-10}$ ($WHz^{-1/2}$)	Time Constant (m)	Size (mm^2)
Silicon bolometer	1.6		3×10^{-5}	8	0.25–0.70
Metal bolometer	2–4	1		10	
Thermistor bolometer	300	1–6		1–8	0.01–10
Germanium bolometer	2–4		0.005	0.4	1.5
Carbon bolometer	2–4		0.03	10	20
Superconducting bolometer (NbN)	15		0.2	0.5	5×0.25
Thermocouples	300		2–10	10–40	0.1×1 to 0.3×3
Thermopiles	300			3.3–10	1–100
Pyroelectrics	300	2–5		10–100†	2×2
Golay cell	300	10	0.6	10–30	10

†Shorter values can be obtained at the expense of NEP (for laser detection).

and secondary pyroelectric effects take place, thereby generating a body electric charge distribution.[25] Materials most often used for these detectors are TGS (triglycine sulfate), DTGS (deuterated TGS), Li_2SO_4, $LiNbO_3$, $LiTaO_3$, and PLZT (lead lanthanum zirconate titanate). TGS is the most used for specialized sensor systems, but has a relatively low Curie point. For higher-temperature operation, usually $LiTaO_3$ or PLZT is used in the general laboratory environment.

The two advantages of the pyreoelectric detector over the other thermal detectors, bolometers, and thermopiles, are its responsivity and its capability of rapid response. The response time and responsivity are traded by choice of the load resistor in the circuit. For instance, with a 100-MΩ load the time constant can be 1 ms and the responsivity 100 V/W, but with a 1-MΩ load the values would be 10 μs and 1 V/W.

Summary of Elemental Thermal Detector Properties

Although the user should contact suppliers for detailed information, this section provides overall property information about thermal detectors. There are several cautions about summary data. Most detectors can be tailored to have somewhat different properties. Improvements have often been made since the publication of these results. Not all parameters are available in all combinations. Table 1 does, however, give the general flavor of the performance of different thermal detectors.

28.3 ARRAYS

Introduction

As pointed out earlier, thermal detector response is governed by the thermal response time, which is the ratio of the pixel heat capacity C to the thermal conductance G of the heat leakage mechanism. High pixel responsivity is associated with high thermal isolation, i.e., low thermal conductance. Thermal detector design is driven by the thermal isolation structure. It is the structure which determines the extent to which the pixel performance can approach the temperature fluctuation noise limit and, ultimately, the background fluctuation noise limit. Given the value of G associated

with the heat loss mechanism, the pixel heat capacity must be designed appropriately to attain the required thermal response time. Response times in the millisecond range are compatible with high thermal isolation; response times in the microsecond range are not. Thus, two-dimensional arrays of thermal detectors which operate at TV frame rates (30 Hz in the United States) are under development for applications in thermal imagers.

Noise Equivalent Temperature Difference

Whereas elemental detectors are usually described by such figures of merit as NEP and D^*, arrays have been described by a noise equivalent temperature difference (NETD) associated with their use in a camera under certain specific conditions. It is defined as the change in temperature of a blackbody which fills the field of view of a pixel of an infrared imaging system that gives rise to a change of unity in the signal-to-noise ratio at the output of the system. The measurement of the NETD should, however, be with the flooding of several pixels to avoid fringing effects and with an SNR (signal-to-noise ratio) well above 1 to obtain good accuracy. The pixel is defined as the subtense of a single element of the array. The NETD can be written in several different forms. Perhaps the simplest is

$$\text{NETD} = \frac{\sqrt{A_d B}}{D^*(dP_d/dT)} \tag{17}$$

where D^* is the specific detectivity, A_d is the area of a single pixel, B is the system bandwidth and (dP_d/dT) represents the change in power on the detector element per unit change in temperature in the spectral band under consideration. This form does not include the system noise, which is often included by the manufacturers in their calculations. In Eq. (17) the change in power with respect to temperature is

$$\frac{dP_d}{dT} = \frac{A_d \tau_o}{4FN^2} \int_{\lambda_1}^{\lambda_2} \frac{dM}{dT} d\lambda \tag{18}$$

where τ_o is the optics transmission, FN is the focal ratio (defined as the effective focal length divided by the entrance pupil diameter), and M is the radiant emittance of the source. This is almost the definition of the specific detectivity. The NETD can also be written in terms of the responsivity $\Re$, since the detectivity and responsivity are related in the following way:

$$D^* = \frac{\sqrt{A_d B}}{P} \frac{V_S}{V_N} = \sqrt{A_d B} \frac{\Re}{V_N} \tag{19}$$

where V_S is the signal voltage at the sensor and V_N is the rms noise voltage of a pixel in the bandwidth B. Therefore

$$\text{NETD} = \frac{V_N}{\Re(\partial P_d/\partial T)_{\lambda_1 - \lambda_2}} \tag{20}$$

The power on the detector is related to the power on the aperture by the optical transmission τ_o. The expression can also be formulated in terms of the source radiance, L

$$\text{NETD} = \frac{4FN^2\sqrt{B}}{D^* \tau_a \tau_o \pi D \Delta\theta (\partial L/\partial T)_{\lambda_2 - \lambda_1}} \tag{21}$$

where D is the diameter of the aperture, $\Delta\theta$ is the angular subtense of a pixel, L is the source radiance, and τ_a is the atmospheric transmission. One last form can be generated by recognizing that, for an isotropic radiator, the radiance is the radiant emittance divided by π:

$$\text{NETD} = \frac{4FN^2V_N}{A_D\tau_a\tau_o\Re(T_S)(\partial M/\partial T)} \tag{22}$$

In this form of the expression for NETD, it is not necessary that the noise be white, nor is it necessary that the noise not include system noise. Whether or not system noise is included should be clearly stated.

Theoretical Limits

Figure 4 illustrates the theoretical limits of thermal arrays having the parameters shown and operating at 300 and 85 K as a function of thermal conductance. The performance of real thermal arrays with those parameters lies on or above the sloping line. As the conductance G is reduced (better thermal isolation), the noise equivalent temperature difference NETD is reduced (improves) until the background limit is reached, when radiant power exchange between the array and the background becomes the dominant heat transfer mechanism. Reducing the detector temperature to 85 K appropriate to a bolometer operating at the transition edge of the high-temperature superconductor $YBa_2Cu_3O_{7-x}$ (YBCO) reduces the NETD by $\sqrt{2}$ and allows the limit to be reached with less thermal isolation (higher G value).

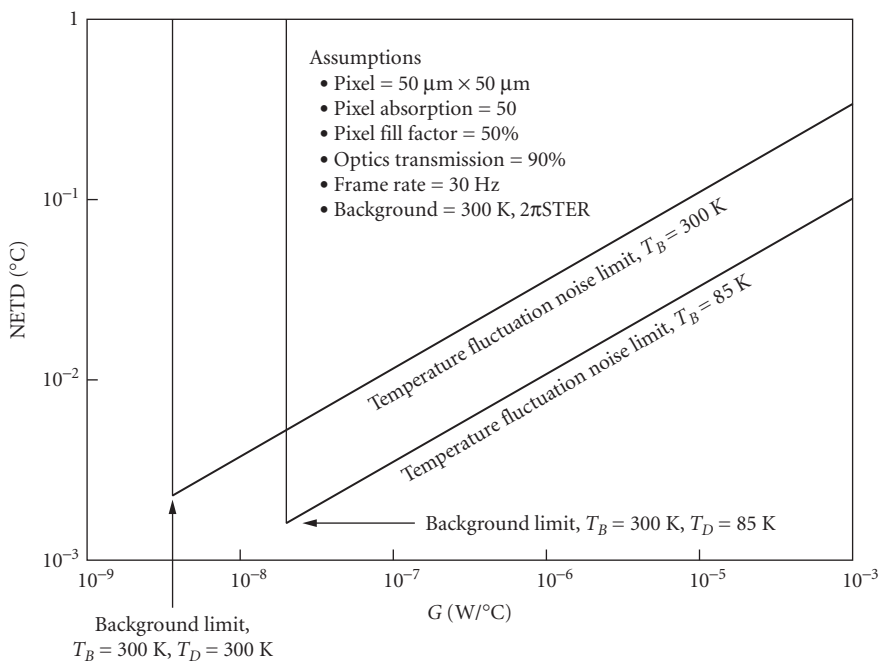

FIGURE 4 Temperature fluctuation noise limit and background fluctuation noise limit of uncooled and cryogenic thermal detector arrays.

Arrays fall into two categories: monolithic and hybrid. Monolithic arrays are prepared on a single substrate, e.g., silicon, upon which the detecting material is deposited in the form of a thin film which is subsequently processed into an array. Hybrid arrays are prepared in two parts: (1) the readout electronics arrays, usually in silicon, and (2) the detecting material array, usually in wafer form which is thinned by lapping, etching, and polishing. These two arrays are mated by a technique such as flip-chip bonding. Here the interconnection at each pixel must have a sufficiently high electrical conductivity, yet a sufficiently low thermal conductivity—a difficult requirement. If array cost considerations are important, then the monolithic approach, especially in silicon, is the more desirable.

Resistive Bolometer Arrays

The development of resistive bolometric arrays has proceeded along two paths: uncooled arrays and cryogenic arrays. Large, uncooled bolometric arrays have been developed at Honeywell by a team lead by R. A. Wood.[26,27] Silicon microstructure technology is employed to produce the arrays, a process resembling the fabrication of integrated circuits. Twelve arrays are prepared on a 4-in-diameter silicon wafer. Each monolithic array consists of 240 × 336 pixels; each pixel is 50 × 50 μm. The detecting material is a thin film of vanadium oxide. A Si_3N_4 membrane having a thermal conductance of 1×10^{-7} WC^{-1} supports the vanadium oxide at each pixel, as shown in Fig. 5. Bipolar transistors implanted in the silicon substrate act as pixel switches for the matrix-addressed array. The response is optimized for the 8- to 14-μm spectral interval. The thermal response time is adjusted for a 30-Hz frame rate. Each pixel is addressed once per frame by a 5-μs pulse. A thermoelectric stabilizer maintains the array at ambient temperature. Other than a one-shot shutter, the camera has no moving parts.

The measured NETD of the camera with F/1 optics at 300 K is 0.04 K. Given the G value of 1×10^{-7} WK^{-1} it can be seen from Fig. 4 that the array is within a factor of 4 of the temperature fluctuation noise limit. Furthermore, the pixel thermal isolation is so complete that there is no measurable thermal spreading among the pixels.

Linear resistive bolometric arrays of the high-temperature superconductor YBCO on silicon microstructures have been prepared by Johnson et al.,[28] also of Honeywell. A two-dimensional array is under development.[29] The monolithic arrays operate at the transition edge from 70 to 90 K. As was true for the uncooled arrays, the superconducting ones employed a silicon nitride membrane to support the thin film and provide thermal isolation. Excess noise at the contacts limited the performance

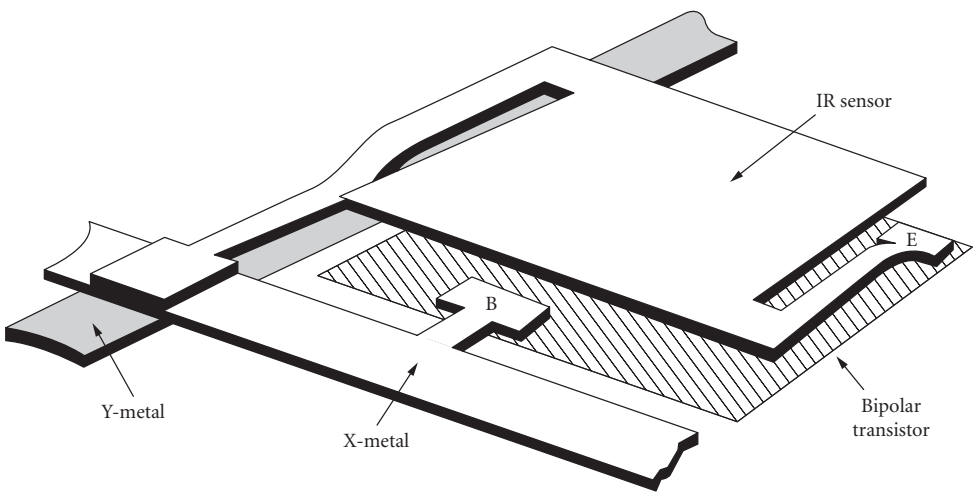

FIGURE 5 Monolithic silicon microbolometer.[26,27] (© *1992 IEEE.*)

of the 12-element linear array. With no excess noise, the calculated NETD[29] of a 240 × 336 array with 50 μm pixels and F/1 optics would be 0.002 K, which is near the 300 K background limit, as shown in Fig. 4.

Pyroelectric Hybrid Arrays

Linear and two-dimensional pyroelectric uncooled arrays have been under development for more than two decades.[20–32] The arrays employ hybrid construction, in which a bulk pyroelectric ceramic material such as lithium tantalate or lead zirconate is mechanically thinned, etched, and polished, then bump-bonded to a silicon substrate containing readout electronics,[33] as shown in Fig. 6. Reticulation is usually employed to prevent lateral heat conduction through the pyroelectric material. The theoretical system NETD of a two-dimensional uncooled array with F/1 optics is estimated to be 0.1 K.[33] Two-dimensional uncooled arrays operating in the 8- to 14-μm region having 100 × 100 pixels, each 100 × 100 μm, are available commercially.[34] Their NETD (with F/1 speed) is 0.35 K. A two-dimensional pyroelectric monolithic array employing a thin film of lead titanate on a silicon microstructure is under development.[35]

Ferroelectric bolometer arrays, also known as field-enhanced pyroelectric arrays, have been developed by Texas Instruments.[36,37] Operation depends upon the temperature dependence of the spontaneous polarization and dielectric permittivity in a ferroelectric ceramic near the Curie temperature. Barium strontium titanate (BST), the selected material, has its composition (barium-to-strontium ratio) adjusted during preparation so the Curie point is 22°C. A thermoelectric stabilizer is employed to hold the BST near 22°C such that the absorbed infrared radiation changes the temperature and thus the dielectric properties. The effect is similar to the pyroelectric effect; however, a voltage is applied to enhance the signal. Construction of this array is naturally similar to that of the pyroelectric array, described above, as shown in Fig. 7. Reticulation of the ceramic is frequently applied to these arrays as well. A radiation chopper is required as both the pyroelectric and ferroelectric effects depend upon the change in temperature. The Texas Instruments BST array,

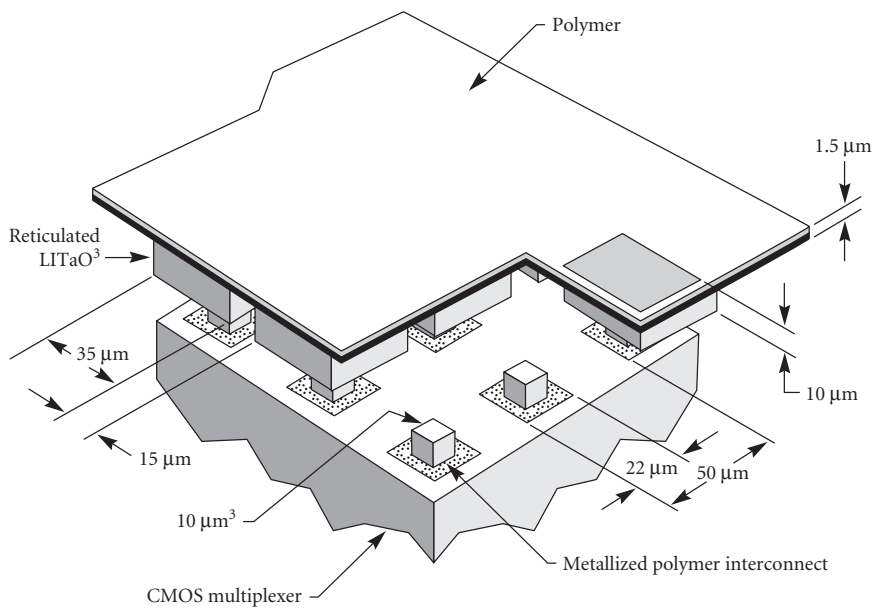

FIGURE 6 Hybrid pyroelectric array structure.[33]

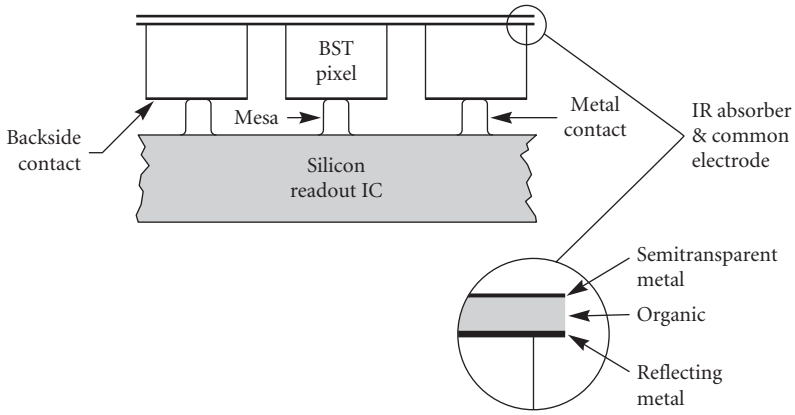

FIGURE 7 Ferroelectric bolometer hybrid array.[36,37]

incorporating 80,000 pixels, each about 50 × 50 μm, which are matrix addressed, has an NETD of less than 0.1°C (with F/1 optics).

Thermoelectric Arrays

Thermoelectric arrays prepared by silicon micromachining have been described by Choi and Wise.[38] Series-connected, thin-film thermocouples, i.e., a thermopile, are prepared on a silicon microstructure, the "hot" junctions (receiving the thermal radiation) on a silicon nitride/silicon dioxide membrane and the "cold" shield junctions on the surrounding silicon substrate. Both 64- and 96-pixel microthermopile linear arrays in silicon microstructures have been prepared by Honeywell,[39] each microthermopile consisting of several nickel iron/chromium thermocouples connected in series, as shown in Fig. 8. The "hot" junctions are deposited on silicon nitride membranes, whereas the "cold" junctions are on the silicon substrates. A camera incorporating the linear array has been employed to image moving targets such as automobiles. With an F/0.73 lens, the measured NETD is 0.10°C.

Since the first publication of this *Handbook*, many advances have been made in these arrays. The suppliers have improved sensitivity somewhat but have increased the number of pixels and decreased their size. The reader should check with the manufacturers for the latest information.

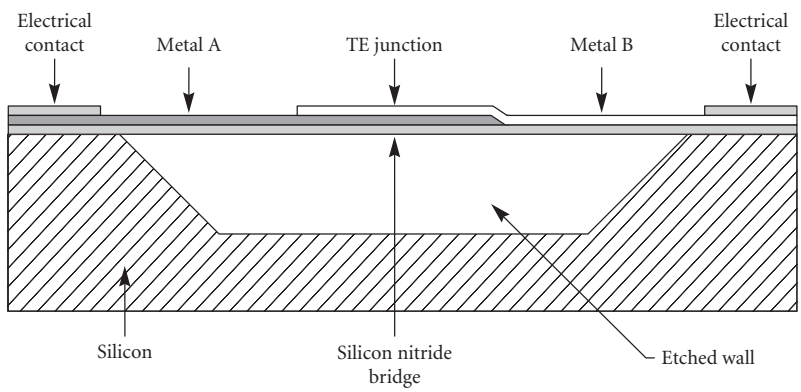

FIGURE 8 Monolithic thermoelectric array.[39] (*© 1991 Instrument Society of America. Reprinted with permission from the Symposium for Innovation in Measurement Science.*)

28.4 REFERENCES

1. P. W. Kruse, L. D. McGlauchlin, and R. B. McQuistan, *Elements of Infrared Technology,* John Wiley and Sons, New York, 1962.
2. R. D. Hudson and J. W. Hudson, *Infrared Detectors,* Halsted Press, New York, 1975; and F. R. Arams, *Infrared to Millimeter Wave Detectors,* Artech House, Dedham, Mass., 1973.
3. E. H. Putley, *Optical and Infrared Detectors,* R. J. Keyes (ed.), Springer-Verlag, Berlin, 1980, chap. 3.
4. R. A. Smith, F. E. Jones, and R. P. Chasmar, *The Detection and Measurement of Infrared Radiation,* Oxford University Press, 1968.
5. R. C. Jones, "The Ultimate Sensitivity of Radiation Detectors," *J. Opt. Soc. Am.* **37:**879 (1974).
6. S. Nudelman, "The Detectivity of Infrared Detectors," *Appl. Opt.* **1:**627 (1962).
7. F. J. Low, "Low Temperature Germanium Bolometer," *J. Opt. Soc. Am.* **51:**1300 (1961).
8. S. Zwerdling, R. A. Smith, and J. P. Thierault, "A Fast High Responsivity Bolometer for the Very Far Infrared," *Infrared Physics* **8:**271 (1968).
9. N. Coron, "Infrared Helium Cooled Bolometers in the Presence of Background Radiation: Optimal Parameters and Ultimate Performance," *Infrared Physics* **16:**411 (1976).
10. N. Coron, G. Dambier, and J. Le Blanc, *Infrared Detector Techniques for Space Research,* V. Manno and J. Ring (eds.), Reidel, Dordrecht, 1972.
11. N. Coron, G. Dambier, J. Le Blanc, and J. P. Moliac, "High Performance, Far Infrared Bolometer Working Directly in a Helium Bath," *Rev. Set Instr.* **46:**492 (1975).
12. W. H. Andrews, R. M. Milton, and W. De Sorbo, "A Fast Superconducting Bolometer," *J. Opt. Soc Am.* **36:**518 (1946).
13. R. M. Milton, "A Superconducting Bolometer for Infrared Measurements," *Chem. Rev.* **39:**419 (1946).
14. N. J. Fuson, "The Infrared Sensitivity of Superconducting Bolometers," *J. Opt. Soc. Am.* **38:**845 (1948).
15. G. Gallinaro and R. Varone, "Construction and Calibration of a Fast Superconducting Bolometer," *Cryogenics* **15:**292 (1975).
16. K. B. Bhasin and V. O. Heinen (eds.), "Superconductivity Applications for Infrared and Microwave Devices," *Proc. SPIE* **1292** (1990). (Includes many other references.)
17. W. S. Boyle and K. F. Rodgers, *J. Opt. Soc. Am.* **49:**66 (1959).
18. D. F. Hornig and B. J. O'Keefe, "Design of Fast Thermopiles and the Ultimate Sensitivity of Thermal Detectors, *Rev. Sci. Instr.* **18:**7 (1947).
19. P. B. Felgett, "Dynamic Impedance and the Sensitivity of Radiation Thermocouples," *Proc. Phys. Soc.* **B62**:351 (1949).
20. M. J. E. Golay, "Theoretical Considerations in Heat and Infrared Detection with Particular Reference to the Pneumatic Detector," *Rev. Sci.* **18:**347 (1947); "Pneumatic Infrared Detector," ibid., **18:**357 (1947); "Theoretical and Practical Sensitivity of the Pneumatic Detector," ibid., **20:**816 (1949).
21. J. R. Hickey and D. B. Daniels, "Modified Optical System for the Golay Detector," *Rev. Sci. Instr.* **40:**732 (1969).
22. M. Chatanier and G. Gauffre, *IEEE Transactions Instr. and Meas. IMEE* **179** (1973).
23. A detector once made by Patterson Moos and cited by R. DeWaard and E. Wormser,"Description and Properties of Various Thermal Detectors, *Proc. IRE* **47:**1508 (1959).
24. E. H. Putley, *Semiconductors and Semimetals,* vol. 5, R. K. Willardson and A. C. Beer (eds.), Academic Press, New York, 1970, chap. 6, "The Pyroelectric Detector;" vol. 12, 1977, chap. 7.
25. Zu-Sheng Wang and Jian-Qi Zhang, "The Mechanism of Type II Pyroelectric Detectors," *Infrared Phys.* **33**(6):481–486 II (1993).
26. R. A. Wood, C. J. Han, and P. W. Kruse, "Integrated Uncooled Infrared Detector Imaging Array," *Proc. of the 1992 IEEE Solid State Sensor and Actuator Workshop,* Hilton Head Island, S.C., pp. 132–135.
27. R. A. Wood, "Uncooled Thermal Imaging with Monolithic Silicon Focal Plane Arrays," *Proc. SPIE* **2020:** Infrared Tech. XIX (1993).
28. B. R. Johnson, T. Ohnstein, C. J. Han, R. Higashi, P. W. Kruse, R. A. Wood, H. Marsh, and S. B. Dunham, "High-T_c Superconductor Microbolometer Arrays Fabricated by Silicon Micromachining," *IEEE Trans. Appl. Superconductivity* **3:**2856 (1993).

29. B. R Johnson and P W. Kruse, "Silicon Microstructure Superconducting Microbolometer Infrared Arrays," *Proc SPIE* **2020:**Infrared Technology XIX (1993).

30. E. H. Putley, "The Pyroelectric Detector," *Semiconductors and Semimetals,* vol. 5, *Infrared Detectors,* R. K. Willardson and A. C. Beer (eds.), Academic Press, New York, 1970.

31. P. A. Manning, D. E. Burgess, and R. Watton, "A Linear Pyroelectric Array IR Sensor," *Proc SPIE* **590:**2 (1985).

32. R. Watton and M. V. Mansi, "Performance of a Thermal Imager Employing a Hybrid Pyroelectric Detector Array with MOSFET Readout," *Proc. SPIE* **865:**79 (1987).

33. N. Butler and S. Iwasa, "Solid State Pyroelectric Imager," *Proc SPIE* **1685:**146 (1992).

34. GEC-Marconi Materials Technology Ltd., 9360 Ridgehaven Court, San Diego, CA 92123.

35. B. E. Cole, R. D. Horning, and P. W. Kruse, "$PbTiO_3$ Deposited by an Alternating Dual-Target Ion-Beam Sputtering Technique," *Ferroelectric Thin Films II*, A. I. Kingon, E. R. Myers, and B. Tuttle (eds.), *Materials Research Society Symposium Proc.,* **243:**185 (1992).

36. C. Hanson, H. Beratan, R. Owen, M. Corbin, and S. McKenney "Uncooled Thermal Imaging at Texas Instruments," *Infrared Detectors: State of the Art, Proc. of SPIE* **1735:**17 (1992).

37. C. M. Hanson, "Uncooled Ferroelectric Thermal Imaging," *Proc. SPIE* **2020:** Infrared Technology XIX (1993).

38. I. H. Choi and K. D. Wise, "A Silicon-Thermopile-Based Infrared Sensing Array for Use in Automated Manufacturing," *IEEE Trans, on Electron Devices* **ED-33:**72 (1986).

39. M. Listvan, M. Rhodes, and M. L. Wilson, "On-Line Thermal Profiling for Industrial Process Control," *Proc. of the Instrument Society of America, Symposium for Innovation in Measurement Science,* Geneva, NY, August 1991.